Structure determination of metastable epitaxial Cu layers on Ag(001) by glancing-incidence x-ray-absorption fine structure

D. T. Jiang, E. D. Crozier, and B. Heinrich
Department of Physics, Simon Fraser University, Burnaby, British Columbia, Canada V5A 1S6
(Received 26 March 1991)

Glancing-incidence x-ray-absorption fine-structure measurements have been performed for an eight-monolayer-thick Cu film epitaxially grown on a Ag(001) surface and covered by an epitaxial ten-monolayer Au film. It is demonstrated that when the top passive layer is a heavier element, but thin, the glancing-incidence technique is still applicable. The x-ray-absorption near-edge structure for this Cu structure is obtained almost free from the distortion due to anomalous dispersion effects and it is different from that of normal fcc Cu. From the extended x-ray-absorption fine-structure analysis, the structure of the Cu film has been determined to be body-centered tetragonal with lattice constants $a = 2.88$ Å and $c = 3.10$ Å, which is 7.6% expanded vertically from a perfect bcc structure.

I. INTRODUCTION

The rapid development of applying the molecular-beam-expitaxy (MBE) technique to generate and stabilize metallic metastable structures has attracted increasing interest in recent years. Under well-controlled MBE conditions, atoms of one element can be deposited onto a suitable template crystal substrate of another element in a layer-by-layer fashion, following a particular atomic registry that does not exist otherwise in nature. In the case of layered $3d$-transition-metal systems, artificial crystalline structures with various interesting magnetic properties have been engineered.[1–5]

To understand thoroughly the properties of the metastable films, it is obviously crucial to characterize the structure in detail. Various surface-structure techniques have been applied in this field. Reflection high-energy electron diffraction (RHEED) is used during the growth to monitor the film thickness,[6] in-plane lattice constants, and symmetry.[7] However, RHEED cannot obtain the lattice spacing perpendicular to the surface, nor can it determine the arrangement of different atomic species in the surface unit cell. X-ray photoelectron diffraction (XPD) (Ref. 8) has been used to determine relative lattice expansions and contractions in the surface-normal direction.[9] It involves intrinsically an electron multiple-scattering process, and consequently it is limited to the study of the top two to four monolayers (ML) of a surface.[10] The quantitative interpretation of low-energy electron-diffraction (LEED) patterns requires a thorough consideration of electron multiple scattering but it is a more established technique and has been applied to some metastable metallic films.[11,12] In the case of Ni on Fe(001), Wang, Li, Jona, and Marcus, using LEED, showed that Ni grows in a pure bcc structure up to 6 ML, but the attempt to decipher the structure of thicker Ni films, which stabilize after 13 ML and retain the same structure up to more than 100 ML, was not successful.[12] In contrast to the complex quantitative analysis of LEED, x-ray-diffraction data can be interpreted by relatively simple kinematic theories. In glancing-angle incidence, the x-ray-diffraction technique has a surface sensitivity that is comparable to other surface techniques.[13] It has been shown to be very powerful in determining the structure of reconstructed surfaces[14–18] when the noninteger indexes of the surface Bragg rods can be easily separated from the bulk signal. In principle, the technique is also applicable to the system of interest here, as was in the glancing-incidence x-ray-diffraction study done on an interface problem by Marra, Eisenberger, and Cho.[19] Conventional x-ray diffraction has also been used in solving the structure of epitaxial metallic thin films in conjunction with other techniques.[20,21]

The technique to be discussed in this paper, extended x-ray-absorption fine structure (EXAFS), has also been applied to epitaxially grown films.[22–26] Being a local atomic structure probe, EXAFS has difficulty in solving a crystal structure independently. But, by the same token, it can provide valuable complementary structural information that is difficult to obtain by the long-range-order diffraction techniques. For example, in the case of Ni (37 ML) on Fe(001), EXAFS showed that the nearest- and the second-nearest-neighbor distances of a Ni atom are identical to those of a fcc Ni atom, and so is the ratio of the coordination numbers of the two atomic shells.[24] This leads to the proposing of a defect-induced model for the observed unusually large fourth-order anisotropy.[2] In a favorable case like 357-Å Co on GaAs (110), Idzerda, Elam, Jonker, and Prinz using total electron detection normal-incidence EXAFS concluded that Co has a metastable bcc structure.[23]

In this paper we present our glancing-incidence x-ray-absorption near-edge structure (XANES) and EXAFS results for a single 8-ML Cu film epitaxially grown on a Ag(001) surface and covered with 10 ML of Au. The structure of the Cu in the Cu/Ag(001) system as determined by using XPD (Ref. 9) and RHEED (Ref. 4) has been reported to be close to bcc. Our EXAFS shows that the Cu is body-centered tetragonal with the c axis (perpendicular to the substrate) being expanded 7.6% relative

to the a axis. This system is important in the context of the magnetic behavior of Fe/Cu/Fe trilayers on Ag(001). Heinrich and co-workers have shown that the exchange coupling depends on the thickness of the Cu interlayer, changing from ferromagnetic to antiferromagnetic for greater than 8 ML of Cu.[4] Theoretical attempts to explain the antiferromagnetism assuming a pure bcc structure of Cu have failed.[27]

The material in this paper is organized as follows. In Sec. II the glancing-incidence EXAFS and associated detection techniques are discussed. Experimental results are presented in Sec. III, followed by the data analysis in Sec. IV. The results are summarized and discussed in Sec. V.

II. EXPERIMENT

In the x-ray region the index of refraction is less than unity by an amount proportional to the electron density. When x rays are incident onto a sample surface, there is a critical angle θ_c below which the x rays undergo total reflection.[28] In this case there exists an evanescent wave confined typically within a penetration depth of 15–30 Å in the surface region of the sample. Reflectivity, diffraction, and EXAFS techniques have used this effect to study surfaces and interfacial regions.

A schematic diagram of the glancing-incidence setup used in this experiment is shown in Fig. 1. The sample was mounted in the plastic chamber of a total electron yield detector,[29] which in turn was spring-loaded on a stepping-motor-driven angular scanning stage.[30] With this arrangement the x-ray incident angle θ (Fig. 1) could be tilted in angular steps of 13.5 μrad and the x-ray fluorescence, reflectivity, and total electron yield could be monitored at the same time. The fluorescence signal was monitored by a wide-aperture ionization chamber filled with argon gas. The incoming beam intensity monitor I_0 and the reflectivity monitor I_r were standard 6-in.- and 12-in.-long ionization chambers, respectively, provided by the Stanford Synchrotron Radiation Laboratory (SSRL), and filled with nitrogen gas.

The incident x-ray beam is first defined by a Huber slit s_1 (Fig. 1) opened horizontally to 5 mm and vertically to 44 μm to accommodate the effective sample size at a tilting angle around 3 mrad. When the sample is inserted into the beam, normally there is a transverse tilt angle of several mrad with respect to slit s_1 due to the construction of the positioning stage on which the sample rests.

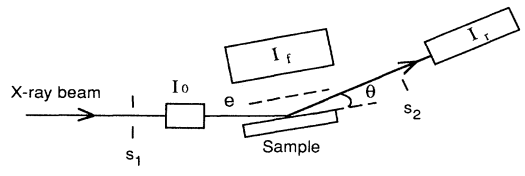

FIG. 1. A schematic diagram of the glancing-incidence EXAFS experimental setup: I_0, I_f, and I_r are ionization chambers; e is the total electron yield detector; s_1 is the Huber slit; s_2 is a beam stop.

Although this transverse angle introduces a negligibly small error in the beam incident angle θ,[30] it can cause a higher background and unwanted Bragg peaks in the detected signal due to part of the crystal substrate being exposed to the direct incident beam. To eliminate this problem, the slit s_1 is mounted on a transverse rotation stage driven by a motor micrometer[31] such that the transverse tilt angle can be adjusted. The beam stop s_2 is also mounted on a similar transverse rotation stage, which is set on a vertical translation stage driven by a stepping motor. A detailed description of the experimental alignment procedure has been given in Ref. 30.

The data were taken on beam line IV-1 at SSRL operating in dedicated mode with SPEAR providing a 3-GeV electron beam at a typical current of 50 mA. A Si(220) double-crystal monochromator was used with the entrance slit set at 0.5 mm. To reduce harmonic contamination in the incident beam the monochromator was detuned above the Cu K edge such that the current reading in the I_0 chamber was 50% of its maximum value.

The sample measured was an 8-ML single-crystal Cu film epitaxially grown in a MBE chamber on a Ag(001) surface, in the form of a disk with 1.5 cm diam. On top of the Cu film a single-crystal Au layer of 10 ML was grown to protect the Cu film from oxidation when it was later taken out of the ultrahigh vacuum for the glancing-incidence EXAFS studies. The detailed procedure of the sample preparation was similar to that described in Ref. 4.

Because both the Au and Cu layers are very thin, the effective critical angle θ_c of the sample is determined mainly by the Ag substrate. In the energy range of Cu K-edge x-ray-absorption fine structure (XAFS), the effective θ_c is about 6.8 mrad. In order to establish the angular scale, the fluorescence, total electron yield, and reflectivity were measured as a function of the incident angle while the photon energy was kept at different constant values below and above the Cu K edge. XAFS spectra were then obtained at angles ranging from $\sim 0.5\theta_c$ to $1.5\theta_c$. While taking the initial spectra, any Bragg peaks and other reproducible suspicious features (e.g., monochromator crystal "glitches"[32]) were located by cross examining the data collected simultaneously in the three methods, and the azimuthal orientation of the sample and the monochromator detuning condition were adjusted to optimize the XAFS signal.

Due to anomalous dispersion, the near-edge structure obtained by total electron yield and reflectivity changes with the incident angle θ, leading to a severe distortion in the near-edge part of the data when θ approaches θ_c. However, the fluorescence signal was found to be independent of the incident angle θ: the background fluorescence signals were mainly from the L edges of the Ag substrate and M edges of the Au cover layer and these relatively low-energy fluorescence photons were stopped by the 0.64-mm-thick Plexiglas cap of the total electron yield detector. In a sense the total electron detector housing acted as a high pass filter for fluorescence photons. As a result, the anomalous dispersion made a very small contribution to the fluorescence signal detected, and its effect was not visible in our data. Calculations

show that the distortion in the near-edge structure of the 8-ML Cu is about 1% of the edge jump at 10 eV above the first inflection point when $\theta \sim \theta_c$, compared with about 20% distortion if the entire fluorescence signal was detected.[33] At incident angles $\theta \leq 0.78\theta_c$, the data obtained from all three detection methods tend to agree. In this paper we analyze the fluorescence data, not only because they are almost free from the anomalous dispersion effect but also a relatively simple way of estimating the correction needed in the EXAFS amplitude and phase is available.[34]

The fact that glancing-incidence EXAFS is observable when Cu is covered with a heavier element Au even at incident angles much smaller than the critical angle is noteworthy. In applications of the glancing-incidence EXAFS technique it is normally stated that a buried film or substrate can only be studied at angles less than its critical angle for total reflection, θ_c, if the θ_c of the covering layer is smaller. But this is not valid for thin covering layers. Calculations indicate that experimentally useful penetration into the Cu layer will occur for covering films of Au up to 30 Å thick.[33]

III. EXPERIMENTAL RESULTS

A. XANES

The x-ray-absorption near-edge structure (XANES) of fcc Cu, 8-ML Cu, and bcc Fe are plotted in Fig. 2(a). The reference data of fcc Cu and bcc Fe were obtained by the transmission method on pinhole free metal foils of thickness 3 μm. The 8-ML Cu data were obtained by averaging the data sets taken in an incident angle range of $0.67\theta_c \leq 0.87\theta_c$ using fluorescence detection. The 8-ML Cu XANES was prepared by first subtracting a linear fit to the preedge background and then normalizing to the linear fit above the edge.

There is a small, but reproducible, shift of the first inflection point of the 8-ML Cu spectrum to 0.16±0.1 eV below that of fcc Cu.

In the XANES of fcc Cu the three peaks in the energy range 0–30 eV have been shown to be well correlated with the positions of energy eigenvalues of X_4', X_5', and L_3' band states.[35] States lying on the Brillouin-zone boundary have a high density of states because the bands are flattened and hence correspond to peaks in the absorption spectrum. However, in the XANES of 8-ML Cu in the same energy range the second and third peaks in fcc Cu are replaced by one broadened peak and the spectrum is different from that of fcc Cu. On the other hand, the XANES of 8-ML Cu is more similar to that of bcc Fe with respect to peak positions and strengths throughout the XANES energy range. The similarities are more evident in the derivative plots shown in Fig. 2(b).

Based on these observations we expected that the 8-ML Cu would have a structure close to that of bcc Fe. The following EXAFS analysis confirmed this. No quan-

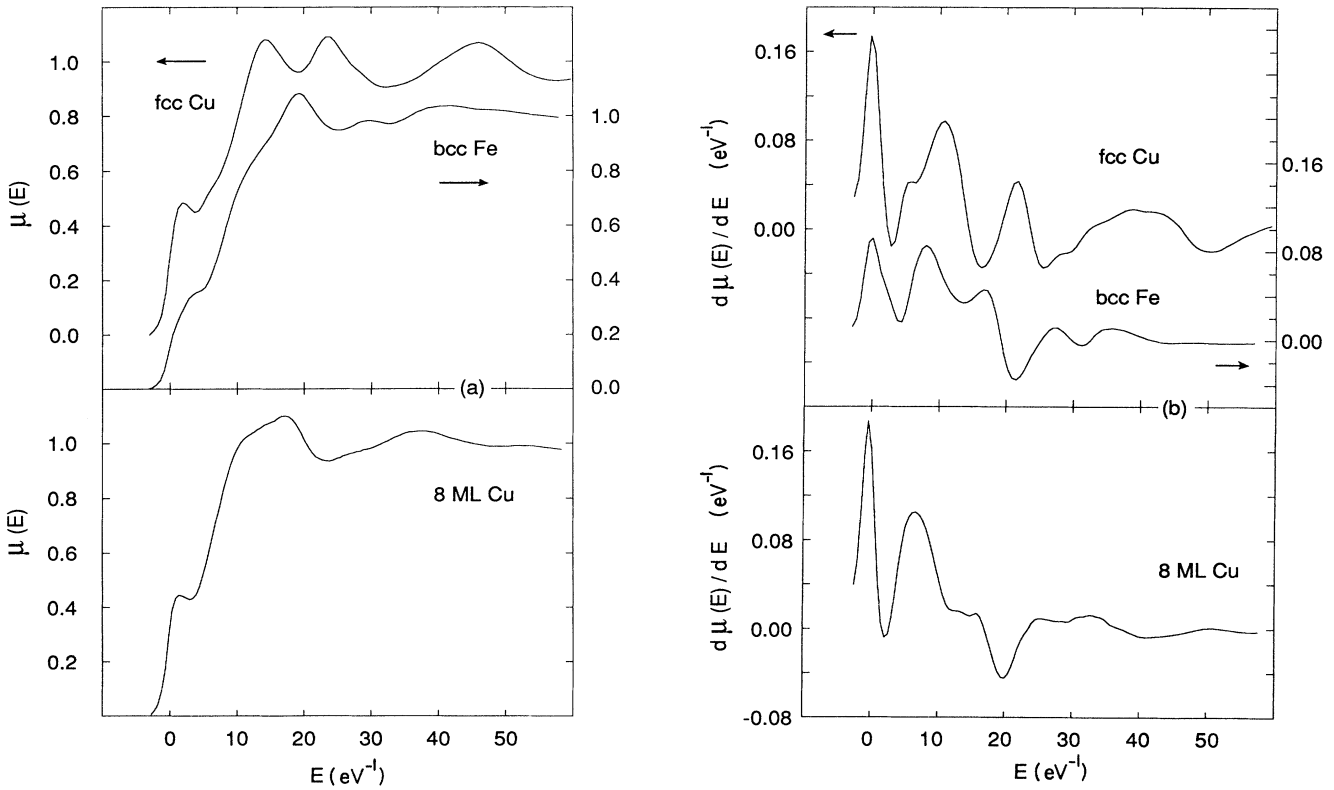

FIG. 2. (a) The XANES spectra of the K edges of bulk samples of fcc Cu, bcc Fe, and of Cu in the epitaxially grown system Au(10 ML)/Cu(8 ML)/Ag(001). The absorption coefficient $\mu(E)$ has been normalized to unity at the edge as per the text. The zero of the energy scale coincides with the first inflection point for each edge. The inflection point for the 8-ML Cu is 0.16 eV below that for fcc Cu. (b) The derivative of the XANES spectra of (a).

titative analysis is attempted here on the XANES of the 8-ML Cu. However, this XANES of a Cu crystal completely different from the natural bulk structure should serve as a good test for the first-principles theoretical calculations of XANES that have been developed to give agreement with fcc Cu.[35–38]

B. EXAFS

The EXAFS interference function is normally defined by $\chi(k)=[\mu(E)-\mu_0(E)]/\mu_0(E)$, where $\mu_0(E)$ is the atomic absorption coefficient. The $\chi(k)$ shown in Fig. 3 were extracted from the raw data by removing the post-edge background by a polynomial fit and normalizing by the edge jump obtained by extrapolation of linear fits in a range of about 30 to 130 eV above the edge. Since the $\chi(k)$ of the 8-ML Cu was eventually curve fitted using empirical amplitude and phase shifts from fcc Cu, a McMaster correction for the energy dependence of the background was not applied.[39] The $\chi(k)$ of 8-ML Cu is limited to the range shown because of the existence of a Bragg peak at 9 Å^{-1}.

The Fourier transforms of $k\chi(k)$ are shown in Fig. 4 using the limited range of the 8-ML Cu data. In the insets of Fig. 4 are shown the transforms of the reference data using a larger k space range. The transforms of 8-ML Cu and bcc Fe show two peaks in the range 1.5–3 Å with a different degree of separation, while the transform of fcc Cu in this range is different. Although one cannot directly assign two atomic shells to the two peaks, it is plausible that there is more than one shell in 8-ML Cu. There is a big difference between the transforms of 8-ML Cu and bcc Fe in the range 4–5 Å. In this range the transform of the bcc Fe is determined by the fourth and fifth nearest neighbors. The fifth nearest neighbor is on the body-center diagonal site; focused multiple scattering causes the peak in the transform to be extraordinarily high (see the inset). The strong dampling of this feature in the transform of 8-ML Cu indicates again the deviation from a regular bcc structure.

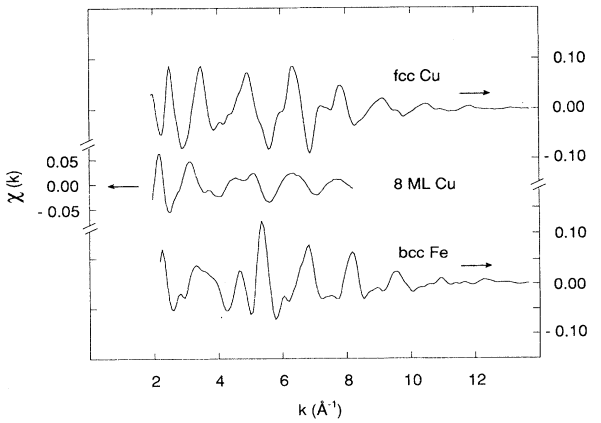

FIG. 3. The EXAFS interference functions $\chi(k)$ of fcc Cu, bcc Fe, and the 8 ML of Cu grown on Ag(001).

IV. DATA ANALYSIS

A. Beating analysis

Considering single scattering and the low disorder limit, the EXAFS interference function $\chi(k)$ can be written as[40]

$$\chi(k)=\sum_j \frac{N_j}{kR_j^2}S_0^2 f_j(k)e^{-2k^2\sigma_j^2}e^{-2R_j/\lambda}\sin[2kR_j+\varphi_j(k)] \tag{1}$$

for N_j atoms at the mean distance R_j from the x-ray-

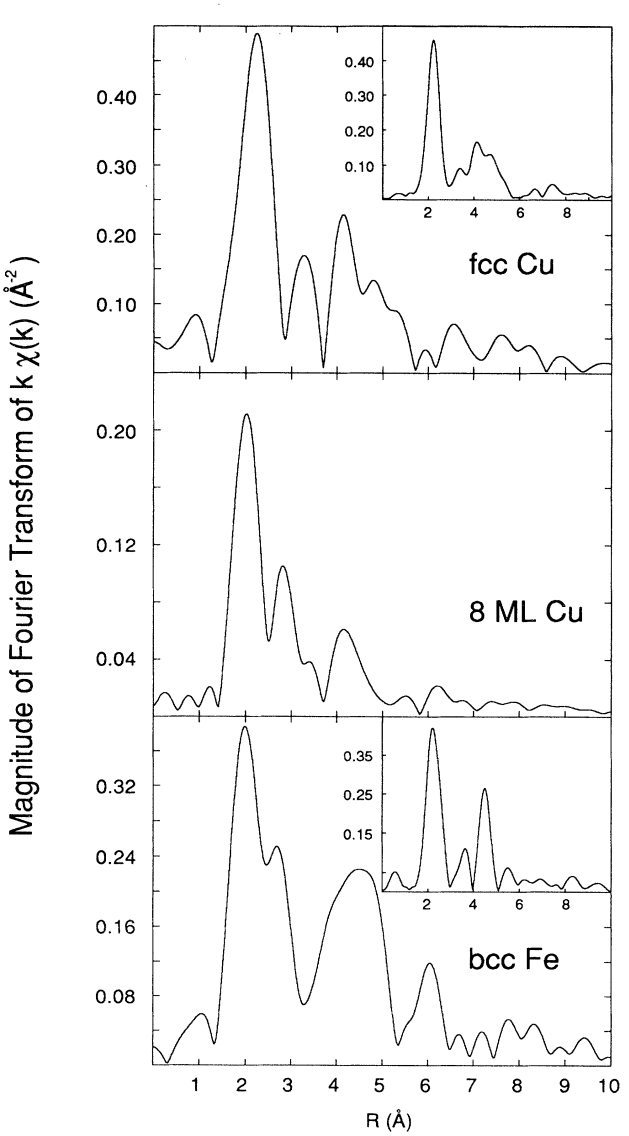

FIG. 4. The magnitude of the Fourier transform of $k\chi(k)$ for fcc Cu (top), 8 ML of Cu (middle), and bcc Fe (bottom). The $\chi(k)$ of Fig. 3 were transformed over the range $2.3<k<8.0$ Å^{-1} using a rectangular window function. The insets show the magnitudes of the Fourier transforms with $k_{\max}=15$ Å^{-1} and a 10% Gaussian window.

absorption atom where σ_j^2, the mean-squared relative displacement in R_j, is due to thermal motion and static disorder. $f_j(k)$ is the magnitude of the backscattering amplitude of the jth-neighbor atom. Many-body effects are included in S_0^2, an amplitude reduction factor representing central atom shake-up and shake-off effects, and in λ, the mean free path of the electron due to the finite core hole lifetime and interactions with the valence electrons. $\varphi_j(k)$ is the sum of the central and backscattering phase shifts. $f_j(k)$ and $\varphi_j(k)$ can either be extracted from a reference system or calculated from first principles.

When two shells have the same atomic species, the EXAFS of the two shells can be written as[41,42]

$$\chi(k)=\frac{1}{k}\tilde{A}(k)\sin[2k\tilde{R}+\tilde{\varphi}(k)] , \tag{2}$$

where

$$\tilde{A}(k)=A_1(k)[1+C^2(k)+2C(k)\cos(k\,\Delta R)]^{1/2} ,$$

$$\tilde{\varphi}(k)=\varphi_1(k)+\tan^{-1}\left[-\frac{1-C(k)}{1+C(k)}\tan(k\,\Delta R)\right] .$$

$A_1(k)$ and $\varphi_1(k)$ are the effective backscattering amplitude and the central plus backscattering phase shift of shell 1, $\tilde{R}=(R_1+R_2)/2$ is the mean bond length of the two shells, $C(k)$ is the ratio of backscattering amplitude of shell 2 over shell 1, and $\Delta R=R_2-R_1$. Due to the interference of the two shells, minima appear in the total backscattering amplitude $\tilde{A}(k)$ and kinks occur in $\tilde{\varphi}(k)$ with values of k at the beating nodes,

$$k_{(2n+1)}\approx\frac{(2n+1)\pi}{2\Delta R}, \quad n=0,1,2,\ldots . \tag{3}$$

One can use $\tilde{A}(k)$ or $\tilde{\varphi}(k)$ to measure the values of $k_{(2n+1)}$ and thus deduce ΔR. In practice, the kink position is located by taking the derivative of the phase with respect to k. The obvious advantage of this method over other analysis techniques is that knowledge of the backscattering amplitude and phase is not needed.

When a large-k-range $\chi(k)$ is available, the beating analysis can quantitatively determine[41] ΔR. This is demonstrated in the case of bcc Fe. In bcc Fe the distance difference between the first two shells is $\Delta R=0.385$ Å.[43] Using a Fourier transform with a k-space transform range of 2–16 Å^{-1} and an R-space backtransform range of 1.42–3.07 Å, the first-order beat node was determined consistently in both the amplitude and phase derivative to be $k_1=4.05\pm0.04$ Å^{-1}, where the error bar was estimated by changing the ranges of the transform windows. Using $k_1\,\Delta R=\pi/2$, we get $\Delta R=0.388\pm0.004$ Å, i.e., an error less than 0.01 Å compared to the exact value.

In the case of the 8-ML Cu film, the k-space data range is limited to about 8 Å^{-1} and consequently the first two shells are not well separated from higher shells in the transform. When Fourier filtering is applied, the transform artifacts and the correlation between the beat node position and quantities like coordination numbers and Debye-Waller factors start to have noticeable effects on the value determined for the beat node. Tests of using the beating analysis on the bcc Fe data over the restricted k-space data range showed that the error in ΔR could be as much as 0.03 Å, depending on the details of the transform procedures. However, if the analysis is applied to the 8-ML Cu and bcc Fe in a systematic way, comparison provides structural information that can then be used as a guideline for a detailed modeling and to check the consistency of results from different analysis techniques.

Using a rectangular window, the Fourier transform of $k\chi(k)$ (Fig. 4) of the 8-ML Cu between 1.38 and 3.35 Å was Fourier filtered and the amplitude and phase were extracted. Figure 5 shows the results for the derivative of the phase as a function of k. For comparison, the results for bcc Fe and fcc Cu, prepared in the same manner, are also shown. The strong beating effect in both bcc Fe and the 8-ML Cu are clearly evident, i.e., similar to bcc Fe the first and second shells of the 8-ML Cu have a small separation. The gradual modification in the low-k part of the derivative of the phase of fcc Cu is probably due to transform artifacts. For the 8-ML Cu the beating node is at 4.52 Å^{-1}; by applying $k\,\Delta R=\pi/2$ we have $\Delta R^{\mathrm{Cu}}=0.348$ Å. Similarly for bcc Fe the node is at 4.25 Å^{-1}, giving $\Delta R^{\mathrm{Fe}}=0.370$ Å, which is 0.015 Å shorter than the exact value. Due to the limited resolution, these numbers depend on the details of the transforms, however the relative beating node separation is meaningful. In Fig. 5 it also can be seen that the depth of the dip in the phase derivative of 8-ML Cu is much smaller than that of bcc Fe. From a detailed modeling study, in which $\chi(k)$ was constructed from Eq. (1), we conclude that the smaller depth of the dip for the Cu is mainly due to a decrease in N_2/N_1 and an increase in $\sigma_2^2-\sigma_1^2$. The mean free path is not important here.

Qualitatively the above beating analysis provides us with the following facts: the 8-ML Cu has a structure somewhat similar to a body-centered one, the bond length difference between the first two coordination shells is shorter than that in bcc Fe, and the quantity

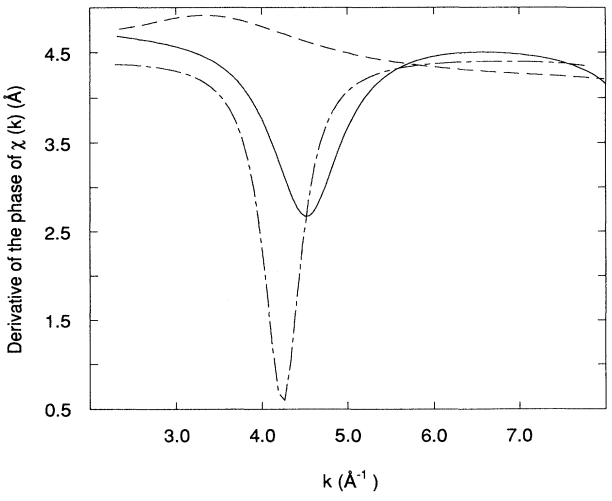

FIG. 5. The phase derivatives of the 8-ML Cu (solid line), bcc Fe (dashed-dotted line), and fcc Cu (dashed line).

$(N_2/N_1)e^{-(\sigma_2^2-\sigma_1^2)}$ of 8-ML Cu is smaller than that of bcc Fe. These are the constraints for the model-dependent analysis discussed in the following.

B. Curve fitting results

To solve the structure quantitatively we applied a nonlinear least-squares curve fitting. The empirical Cu scattering amplitude and phase were extracted from bulk transmission data using the conventional Fourier filtering technique. The directly extracted empirical EXAFS amplitude function was $(1/kR_1^2)N_1S_0^2f(k)e^{-2\sigma^2k^2}e^{-2R_1/\lambda}$, which was multiplied by kR_1^2/N_1 to get the effective atomic scattering amplitude $S_0^2f(k)e^{-2\sigma^2k^2}e^{-2R_1/\lambda}$. The R_1 and N_1 used for fcc Cu were 2.556 Å and 12.[43] This means that we neglected any possible differences between the values for S_0^2 and λ in bulk and in the thin-film state. The ΔE_0 was always fixed at 0.

The $k^3\chi(k)$ $(2.85 \le k \le 7.42$ Å$^{-1})$ of 8-ML Cu was Fourier transformed using a 10% Gaussian window and the curve fitting was applied to its Fourier transform in R space within the range $0.8 \le R \le 2.8$ Å. Four parameters were varied: the nearest- and the second-nearest-neighbor bond lengths, R_1 and R_2, and the corresponding mean-squared-relative displacements σ_1^2 and σ_2^2. The result is listed in Table I, where

$$\Delta\sigma_i^2=\sigma_{i\text{8-ML Cu}}^2-\sigma_{\text{fcc Cu}}^2 .$$

The uncertainties of the results were determined by finding that deviation of a parameter from its best-fit value which doubles the residual sum of squares,

$$\sum_{i=1}^{N}(\text{Data}_i-\text{Fit}_i)^2/\sigma_{\text{stat}(i)}^2 ,$$

where $n_{\text{free}}=1+2\,\Delta k\,\Delta R/\pi$, n is the number of fit parameters, and $\sigma_{\text{stat}(i)}^2$ is the statistical standard deviation of the data, meanwhile allowing all other $(n-1)$ variables to float. The error bar defined in this way could be too conservative,[39] possibly by as much as a factor of 2.[44] The coordination numbers were fixed to reduce the intercorrelation between varying parameters to an acceptable level. The values of N_1 and N_2 in Table I are those for a perfect bcc structure. The results of R_1 and R_2 were not sensitive to the changes in N or σ^2: varying N_1 between 7 and 8 and N_2/N_1 between 0.60 and 0.75 gave essentially the same results for the R's. When all the parameters were allowed to float, the results for the bond lengths remained within the error bars quoted in Table I, but the residual sum of squares was two or three times larger.

Figure 6 shows the magnitude and the imaginary part of the Fourier transform of $k^3\chi(k)$ of the 8-ML Cu and the fit using the parameters in Table I. The vertical dashed line at 2.8 Å in the graph indicates the upper bound of the fitting range. Beyond this line, the effect of multiple scattering from the nearest-neighbor triangular path becomes appreciable and is not included in our single-scattering approximation.

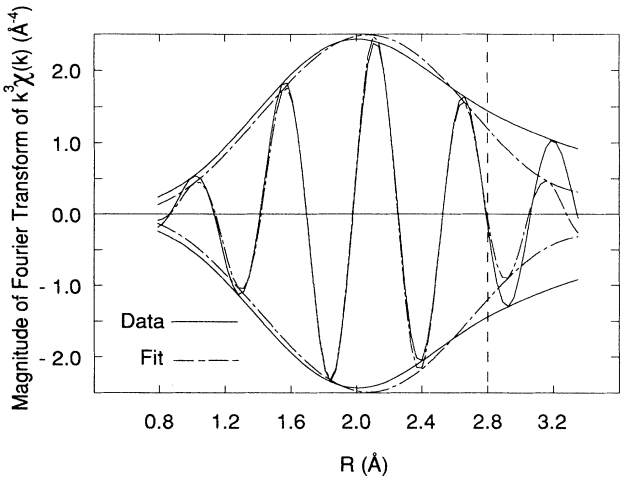

FIG. 6. R-space curve fitting of 8-ML Cu. The vertical dashed line at 2.8 Å indicates the upper limit of the fitting range, above which the contribution of multiple scattering from the nearest-neighbor triangular path is significant.

TABLE I. Results of fitting the Cu K-edge EXAFS spectrum. Fixed parameters: $\Delta E_0=0$, $N_1=8$, $N_2/N_1=0.75$.

R_1 (Å)	$\Delta\sigma_1^2$ (10^{-3} Å^2)	R_2 (Å)	$\Delta\sigma_2^2$ (10^{-3} Å^2)
2.56±0.02	1.8±2.7	2.88±0.036	$5.8^{+6.9}_{-4.7}$

As can be seen from Table I, the difference between the two shells is 0.32±0.04 Å, which is consistent with the result of 0.348 Å obtained from the beating analysis discussed earlier.

In our experimental arrangement, the polarization direction of the incoming synchrotron radiation was parallel to the (001) surface of the sample. For a perfect cubic structure there is no polarization dependence in the spectrum.[45] However, it will be shown in the following section that the results in Table I lead to a tetragonal structure with its c axis along the sample surface normal. This departure away from a perfect bcc structure causes the angle between the first-nearest-neighbor bond and the (001) surface normal to be 52.74°, which is about 2° less than the magic angle[46] in a bcc case. Using the formulas in Ref. 46, reductions in the effective coordination numbers for the first and second shells are calculated to be 5% and 0%, respectively. Besides the polarization effect, the residual anomalous dispersion effect will also cause a reduction in the effective coordination number and, in addition, a small constant EXAFS phase shift.[34] It can be shown that the effect becomes less important as the film becomes thinner.[33] In our particular case of 8-ML Cu, the effective coordination number reduction is only about 3% when $\theta<\theta_c$ and the additional constant phase shift is less than 0.06 rad for any incident angle. Both the amplitude and phase corrections are practically independent of photon energy in the EXAFS range. With these amplitude and phase corrections implemented, the fitting result for R_1,R_2 and the residual sum of squares essentially

remain the same as the values in Table I, but $\Delta\sigma_1^2$ and $\Delta\sigma_2^2$ are changed to 0.5×10^{-3} and 6.5×10^{-3}, respectively.

V. DISCUSSION

The fcc Ag(001) surface rotated 45° can be viewed as a primitive square lattice with a transverse lattice constant $a_{Ag}/\sqrt{2}=2.89$ Å, where $a_{Ag}=4.09$ Å is the lattice constant of fcc Ag. It is known from the RHEED study that the transverse lattice in the Cu film has fourfold symmetry and has a transverse lattice constant very close to that of the square Ag atom array.[4] To minimize the surface free energy, the logical sites for the first monolayer Cu atoms are the fourfold symmetry hollow sites in the center of the square cornered by four Ag atoms, which are the minima of the substrate-induced periodic potential. For the same reason, the second and the following Cu layers should also grow on the fourfold symmetry sites. This process leads us to have either body-centered-cubic, face-centered-cubic, or tetragonal lattices, depending only on the length of the lattice constant c along the surface-normal direction. If c equals the transverse lattice constant a', the structure is bcc; if $c=\sqrt{2}a'$, it is fcc; and in all the other cases it is tetragonal. In our experiment the polarized incident synchrotron radiation had its electric vector parallel to the sample surface, so the bonds of length $R=c$ in the normal direction were not detected. Therefore, there was no need to include another shell very close to the second nearest neighbor in the fitting. The second-nearest-neighbor distance $R_2=2.88$ Å then is equal to the transverse lattice constant a'. Although this square lattice has a 20% lattice mismatch with fcc Cu (lattice constant[43] $a_{Cu}=3.615$ Å), the lateral atomic registry on the Ag surface is conserved. In this regard the EXAFS result essentially agrees with that from RHEED. The vertical lattice constant in a body-centered tetragonal is $c=(4R_1^2-2R_2^2)^{1/2}$. From the data in Table I we have $c=3.10\pm0.09$ Å, where the error bar is deduced from those of R_1 and R_2. So based on the fitting analysis we conclude that the 8-ML Cu has a body-centered-tetragonal lattice with $c/a=1.076\pm0.043$, i.e., it is (7.6±4.3)% expanded from a bcc structure along the surface-normal direction. The error bars were estimated conservatively and represent an overestimate.

To this point our structural conclusions are based only on EXAFS data. If we assume the transverse lattice constant of 2.90 Å as measured with RHEED and assume a bcc structure, then the nearest-neighbor distance would be 2.515 Å, which is significantly smaller than the value $R_1=2.56\pm0.02$ Å determined from EXAFS. The value of R_1 in bct is the same as in fcc Cu ($R_1=2.556$ Å), but the atomic volume for bct is 9% larger than for fcc Cu.

Using XPD, Egelhoff and Jacob reported that the vertical expansion of Cu on Ag(001) surface is about 4%.[9] The sample in the XPD study had 6.5-ML Cu on Ag(001) and no covering material on top of it. It has been observed that around 8 ML during the growth the LEED became slightly smeared.[47] The expansion obtained by the glancing-incidence EXAFS is somewhat larger. This may be due to differences between the samples studied.

Since the glancing-incidence XAFS technique averages over all of the Cu atoms in the sample and the growth of Cu on Ag is not thermodynamically favorable [the surface free energy of Cu is slightly higher than that of Ag (Ref. 48)], the possibility of interdiffusion at the interfaces must be considered. If during the growth of the first few monolayers of Cu on Ag the adsorbed atoms were agglomerated or intermixed with the substrate atoms, the RHEED intensity oscillations would not start from the first monolayer deposited.[49,50] However for the sample used in this study the RHEED intensity oscillations were observed from the beginning to the end of the growth of Cu layers. A similar structure of Cu epitaxially grown on Ag(001) has been studied by XPD,[9] which is an effective technique for detecting surface alloying or interdiffusion:[51] no interdiffusion was reported. For the interface between the Au cover layer and the Cu film the intermixing of the two elements is more unlikely. This growth is thermodynamically favorable from the surface-free-energy point of view and the result from a photoemission study on a Au/Cu(bulk polycrystal) interface indicates that no interdiffusion is observed.[52] This is supported by our RHEED measurements during the growth of the Au overlayer. Cu grows in a simple square lattice while Au shows a complex reconstruction corresponding to a corrugated (111) surface layer of epitaxial Au(001). It is expected that intermixing would affect the characteristic reconstruction of Au. Since the reconstruction was not affected it seems that the interdiffusion is unlikely.

To assess the sensitivity of EXAFS to interdiffusion we have considered two models for the EXAFS interference function $\chi(k)$. The first model assumed a perfect epitaxial structure Au(001)/8 ML of bct Cu/Ag(001). In this case, the Cu in the bottom layer has four Ag atoms as nearest neighbors and four nearest-neighbor Cu atoms and the Cu in the top layer has four Au nearest neighbors and four Cu nearest neighbors. Averaging over the 8 ML of Cu, the effective nearest-neighbor coordination of Cu becomes 7.0 Cu, 0.5 Au, and 0.5 Ag. The second model assumed that diffusion occurs, with the top and bottom layers of Cu interchanging completely with the interfacial Au and Ag layers, respectively, without altering the structure or lattice parameters. The effective nearest-neighbor coordination number for Cu becomes 5 Cu, 1.5 Au, and 1.5 Ag. Both models $\chi(k)$ were fitted under the assumption that Cu has only Cu atoms as nearest neighbors. The second model gave χ^2, the residual sum of squares of errors, that was a factor of 5 larger than for the first model and could be safely rejected. However, it would be difficult to distinguish the first model from the case in which Cu had only Cu as nearest neighbors. Based on these discussions we rule out the possibility of severe interdiffusion in our sample.

Our study of the 8-ML Cu film is relevant to the magnetic behaviors of Fe/Cu/Fe trilayers on Ag(001). Heinrich has shown that the exchange coupling depends on the thickness of the Cu interlayer, changing from ferromagnetic to antiferromagnetic for greater than 8 ML of Cu.[4] Recently an *ab initio* calculation was carried out by Herman, Sticht, and Schilfgaarde on the magnetic prop-

erties of Fe/Cu superlattices assuming a perfect bcc Cu in the film and the result did not reproduce the sign change in the magnetic coupling between Fe layers with different Cu layer thickness.[27] It would be quite interesting to see whether the tetragonal model suggested in this study can provide some further clue for the understanding of the physical mechanism of the oscillatory magnetic coupling.

In conclusion, we have applied glancing-incidence XAFS to a buried single-crystal Cu film only 8 ML thick. It is demonstrated that when the top passive layer is a heavier element, but thin (10 ML in this case), the glancing-incidence technique is still applicable. When the film of interest has a thickness of a few monolayers, such as the case here, the anomalous dispersion effects in fluorescence yield can be eliminated by filtering out the signal from the substrate and the covering layer. This makes it possible to get practically distortion-free XANES without complicated data processing, which would need detailed knowledge of the optical parameters of every layer. The XANES obtained for this Cu structure is strikingly different from that for normal fcc Cu. This XANES of a Cu crystal completely different from the natural bulk structure should serve as a good test for the first-principles theoretical calculations of XANES of Cu metal.

From detailed EXAFS analysis, we conclude that the structure of the 8-ML Cu film is body-centered tetragonal with lattice constants $a=2.88$ Å and $c=3.10$ Å, with the c axis (perpendicular to the substrate) being expanded 7.6% relative to the bcc structure.

ACKNOWLEDGMENTS

We wish to acknowledge the assistance of Z. Celinski and K. Myrtle in preparing the MBE sample. The research was supported by grants from the Natural Sciences and Engineering Research Council, Canada. The Stanford Synchrotron Radiation Laboratory is supported by the U.S. Department of Energy, the Office of Basic Energy Sciences, and the National Institute of Health, Biotechnology Resource Program, Division of Research Resources.

[1]M. N. Baibich, J. M. Broto, A. Fert, F. Nguyen Van Dau, F. Petroff, P. Eitenne, G. Creuzet, A. Friederich, and J. Chazelas, Phys. Rev. Lett. **61**, 2472 (1988).

[2]B. Heinrich, J. F. Cochran, A. S. Arrott, S. T. Purcell, K. B. Urquhart, J. R. Dutcher, and W. F. Egelhoff, Jr., Appl. Phys. A **49**, 473 (1989).

[3]J. J. Krebs, P. Lubitz, A Chaiken, and G. A. Prinz, Phys. Rev. Lett. **63**, 1645 (1989).

[4]B. Heinrich, Z. Celinski, J. F. Cochran, W. B. Muir, J. Rudd, Q. M. Zhong, A. S. Arrott, K. Myrtle, and J. Kirschner, Phys. Rev. Lett. **64**, 673 (1990).

[5]Z. Celinski, B. Heinrich, J. F. Cochran, W. B. Muir, A. S. Arrott, and J. Kirschner, Phys. Rev. Lett. **65**, 1156 (1990).

[6]S. T. Purcell, A. S. Arrott, and B. Heinrich, J. Vac. Sci. Technol. B **6**, 794 (1988).

[7]E. Bauer, in *Techniques of Metals Research,* edited by R. F. Bunshah (Wiley Interscience, New York, 1969), Vol. 2, p. 201.

[8]See, for example, W. F. Egelhoff, Jr., Phys. Rev. B **30**, 1052 (1984).

[9]W. F. Egelhoff, Jr., I. Jacob, J. M. Rudd, J. F. Cochran, and B. Heinrich, J. Vac. Sci. Technol. A **8**, 1582 (1990).

[10]W. F. Egelhoff, Jr., Phys. Rev. Lett. **59**, 559 (1987).

[11]P. A. Montano, Y. C. Lee, J. Marcano, and H. Min, in *Layered Structures and Epitaxy,* edited by J. M. Gibson, G. C. Osbourn, and R. M. Tromp, MRS Symposia Proceedings No. 56 (Materials Research Society, Pittsburgh, 1986), p. 183.

[12]Z. Q. Wang, Y. S. Li, F. Jona, and P. M. Marcus, Solid State Commun. **61**, 623 (1987).

[13]See, for example, M. Nielsen, Z. Phys. B **61**, 415 (1985).

[14]I. K. Robinson, Phys. Rev. Lett. **50**, 1145 (1983).

[15]I. K. Robinson, in *The Structure of Surfaces,* edited by M. A. Van Hove and S. Y. Tong (Springer, New York, 1984), p. 60.

[16]J. Bohr, R. Feidenhans'l, M. Nielsen, M. Toney, R. L. Johnson, and I. K. Robinson, Phys. Rev. Lett. **54**, 1275 (1985).

[17]P. H. Fuoss, D. W. Kisker, G. Renaud, K. L. Tokuda, S. Brennan, and J. L. Kahn, Phys. Rev. Lett. **63**, 2389 (1989).

[18]M. Sauvage-Simkin, R. Pinchaux, J. Massies, P. Claverie, J. Bonnet, N. Jedrecy, and I. K. Robinson, Surf. Sci. **211/212**, 39 (1989).

[19]W. C. Marra, P. Eisenberger, and A. Y. Cho, J. Appl. Phys. **50**, 6927 (1979).

[20]S. M. Durbin, L. E. Berman, B. W. Batterman, M. B. Brodsky, and H. C. Hamaker, Phys. Rev. B **37**, 6672 (1988).

[21]B. T. Jonker, J. J. Krebs, and G. A. Prinz, Phys. Rev. B **39**, 1399 (1989).

[22]D. T. Jiang, N. Alberding, A. J. Seary, and E. D. Crozier, J. Phys. (Paris) Colloq. **47**, C8-825 (1986).

[23]Y. U. Idzerda, W. T. Elam, B. T. Jonker, and G. A. Prinz, Phys. Rev. Lett. **62**, 2480 (1989).

[24]D. T. Jiang, N. Alberding, A. J. Seary, B. Heinrich, and E. D. Crozier, Physica B **158**, 662 (1989).

[25]Y. U. Idzerda, B. T. Jonker, W. T. Elam, and G. A. Prinz, J. Appl. Phys. **67**, 5385 (1990).

[26]H. Oyanagi, T. Fukui, T. Matsushita, T. Yao, T. Ishiguro, H. Saito, and K. Sugii, Physica B **158**, 694 (1989).

[27]F. Herman, J. Sticht, and M. Van Schilfgaarde (unpublished).

[28]L. G. Parratt, Phys. Rev. **95**, 359 (1954).

[29]D. T. Jiang and E. D. Crozier, Nucl. Instrum. Methods A **294**, 666 (1990).

[30]D. T. Jiang, N. Alberding, A. J. Seary, and E. D. Crozier, Rev. Sci. Instrum. **59**, 60 (1988).

[31]ORIEL Encoder Mike™ Actuator, Model 18212, ORIEL Corp., Stratford, CT.

[32]K. R. Bauchspiess and E. D. Crozier, in *EXAFS and Near Edge Structure III,* edited by K. O. Hodgson, B. Hedman, and J. E. Penner-Hahn (Springer-Verlag, Berlin, 1984), p. 514.

[33]D. T. Jiang and E. D. Crozier (unpublished).

[34]S. M. Heald, H. Chen, and J. M. Tranquada, Phys. Rev. B **38**, 1016 (1988).

[35]R. C. Albers, A. K. McMahan, and J. E. Müller, Phys. Rev. B **31**, 3435 (1985).

[36]J. E. Müller and W. L. Schaich, Phys. Rev. B **27**, 6489 (1983);

J. E. Müller and J. W. Wilkins, *ibid.* **29**, 4331 (1984).
[37]J. J. Rehr, R. C. Albers, C. R. Natoli, and E. A. Stern, Phys. Rev. B **34**, 4350 (1986).
[38]G. N. Greaves, P. J. Durhan, G. Diakun, and P. Quinn, Nature **294**, 139 (1981).
[39]F. W. Lytle, D. E. Sayers, and E. A. Stern, Physica B **158**, 701 (1988).
[40]See, for example, E. D. Crozier, R. Ingalls, and J. J. Rehr, in *X-Ray Absorption: Principles, Techniques of EXAFS, SEXAFS and XANES,* edited by D. C. Koningsberger and R. Prins (Wiley, New York, 1988), p. 373.
[41]G. Martens, P. Rabe, N. Schwentner, and A. Werner, Phys. Rev. Lett. **39**, 1411 (1977).
[42]T. Sasaki, T. Onda, R. Ito, and N. Ogasawara, Jpn. J. Phys. **25**, 640 (1986).
[43]R. W. G. Wyckoff, *Crystal Structures,* 2nd ed. (Wiley, New York, 1963), Vol. 1.
[44]K. R. Bauchspiess, Ph.D. thesis, Simon Fraser University (1990).
[45]E. A. Stern, in *X-Ray Absorption,* edited by D. C. Koningsberger and R. Prins (Wiley, New York, 1988), p. 26.
[46]J. Stöhr, in *X-Ray Absorption* (Ref. 45), p. 487.
[47]W. F. Egelhoff, Jr. (private communication).
[48]A. R. Miedema and J. W. F. Dorleijn, Surf. Sci. **95**, 447 (1980).
[49]D. A. Steigerwald and W. F. Egelhoff, Jr., Surf. Sci. **192**, L887 (1987).
[50]W. F. Egelhoff, Jr. and I. Jacob, Phys. Lett. **62**, 921 (1989).
[51]D. A. Steigerwald and W. F. Egelhoff, Jr., Phys. Rev. Lett. **60**, 2558 (1988); W. F. Egelhoff, Jr., CRC Crit. Rev. Solid State Mater. Sci. **16**, 3 (1990).
[52]T. K. Sham and J. Hrbek (private communication).